Protection and Control of Modern Power Systems

ORIGINAL RESEARCH Open Access

Incorporating microgrids coupling with utilization of flexible switching to enhance self-healing ability of electric distribution systems

Saeed Mousavizadeh[1], Arman Alahyari[2*], Seyed Reza Movahhed Ghodsinya[3] and Mahmoud-Reza Haghifam[1]

Abstract

Electric distribution networks have to deal with issues caused by natural disasters. These problems possess unique characteristics, and their severity can make load restoration methods impotent. One solution that can help in alleviating the aftermath is the use of microgrids (MGs). Employing the cumulative capacity of the generation resources through MG coupling facilitates the self-healing capability and leads to better-coordinated energy management during the restoration period, while the switching capability of the system should also be considered. In this paper, to form and schedule dynamic MGs in distribution systems, a novel model based on mixed-integer linear programming (MILP) is proposed. This approach employs graph-related theories to formulate the optimal formation of the networked MGs and management of their proper participation in the load recovery process. In addition, the Benders decomposition technique is applied to alleviate computability issues of the optimization problem. The validity and applicability of the proposed model are evaluated by several simulation studies.

Keywords: Load restoration, Distribution network, Microgrids coupling, Benders decomposition

1 Introduction

In recent decades, natural catastrophes such as hurricanes and floods have caused significant problems for electrical power systems, and some even resulted in large blackouts [1]. This highlights the need to incorporate more resilience into the different sections of power systems [2]. An electrical network should be able to quickly restore its loads in the case of a severe event using an efficient restoration strategy. Some restoration strategies are introduced in [3], and approaches to acquire faster detection of outages are described in [4]. The phenomena that can lead to significant outages and their impacts on the power systems have been studied thoroughly. Each of the studies addresses a particular aspect, including predicting outages, designing corrective actions, strengthening network structure, and providing appropriate restoration plans [5, 6]. With the evolution of the smart grid and the emerging concept of local electricity markets in distribution voltage levels, expectations on electric distribution system are rising substantially [7]. However, because of the weak structure and distinct characteristics of distribution networks such as long feeders, radial topology, and diversity of the components, they are more vulnerable to such incidents.

Among the possible solutions to enhance self-healing in distribution networks, distributed generation (DG) and MGs are considered as effective remedies [8–11]. The advantages for restoration of such options have been extensively reported in the literature. These studies can be divided into three categories. In the first category, recovering the loads after the occurrence of low-impact events is examined, and different approaches are proposed accordingly [12–14]. These studies mainly focus

* Correspondence: Arman.Alahyari@skoltech.ru
[2]Skolkovo Institute of Science and Technology (Skoltech), Moscow, Russia
Full list of author information is available at the end of the article

on changing the network configuration and switching operation after the event in order to reconnect the interrupted segments to the main network [15]. The existing techniques perform satisfactorily in the fault-isolation phase aimed at recovering the maximum loads, though they confront serious difficulties in dealing with major events that have a different nature than the typical faults. Consequently, after high-impact events, the system's desired functionality cannot be achieved by employing the conventional restoration methods. In the second group of studies, MGs are presented as eligible resources to restore the loads after severe disasters [16–20]. However, in these studies, the MG servicing areas are predetermined while their formations during the failure period are not addressed.

The third category includes studies that consider coupling options for MGs. Reference [21] investigates the capability of coupled MGs to act as distributed systems to improve resilience during severe events. A service restoration method is proposed in [22] which uses MGs with limited generation resources to recover critical loads after an extreme event. In [23], the concept of autonomous MG coupling is investigated for improving resilience. Similarly, MG coupling is used in [24] for optimal restoration with the objective function of maximizing the restored critical load. However, in these studies, the network topological characteristics and the switching limitations are not adequately addressed.

The formation of MGs with proper switching operation is studied in [11, 25, 26], while [25] proposes a linear model regarding MG formation after the occurrence of events in the distribution systems. However, the use of tie lines and employing different configurations are not considered. In [11], based on a second-order integer programming approach, a model is proposed to study the impact of reconfiguration capabilities on the load restoration process, though the number of formable MGs and the master generation units, and the dominant controllers in each MG, are predetermined and fixed.

The coupling of the formed MGs and their load sharing during the failure period have not been studied. In addition, the modeling of different types of switches (flexible or non-flexible) and their operational constraints in the recovery process have not been adequately addressed. Inadequate modeling of the switching capabilities can unfold several issues in obtaining measures required for system performance improvement in critical conditions. Thus "failure duration", which has not been included in the proposed models in previous studies needs to be considered.

In this study, by presenting a linear path-based model, the mentioned shortcomings are conveyed, and the topological features of distribution networks and DGs' master controlling potentialities are addressed. In the proposed approach, the formation and the optimal scheduling of the networked MGs are addressed in the form of a linear optimization problem. The time-related features of the events are included and various switching capabilities for coupling the formed MGs during the failure period are considered. Benders' decomposition approach is also used to increase the computability and enhance the efficiency of the methodology. In summary, the main contributions of the paper are as follows:

- The MG coupling concept is used with flexible switches to enhance the self-healing capability of electrical distribution grids.
- A MILP model is proposed and Benders' decomposition is used to optimally schedule the networked MGs
- It considers the time-related features of the flexible switches.
- Several possible strategies are provided and compared using two case studies. The proposed solution methodology is also compared with similar recent studies.

The remainder of the paper is as follows. In Section 2, the advantages of MG coupling in the self-healing process and the required switching capabilities are discussed. The proposed framework for load restoration is described and formulated in Section 3. In Section 4, several simulation studies are presented, and finally, the paper is concluded in Section 5.

2 MGs coupling benefits

In this study, the methods to form dynamic MGs and schedule to reconnect them after a severe event are presented. At peak hours, each formed MG is only capable of providing its own loads, while for other times, by coupling the MGs and aggregating the resources, other loads can also be supplied. Thus, by considering the coupling option, maximum benefits can be accomplished during the recovery process. However, special switching devices are required for implementing such a capability. The switches in distribution networks are considered to be of two different types: flexible and non-flexible. Non-flexible switches are the ones whose open or closed status remains unchanged in the study period.

In contrast, changing the operation modes of the flexible type switches is conceivable during the period while considering the technical constraints.

The example shown in Fig. 1 considers that *T1* and *T4* are flexible switches, *T2* and *T3* are non-flexible, and *MG1* and *MG2* can only supply their own loads at peak hours. Thus, to ensure the power balance constraint in the MGs, flexible switches *T1* and *T4* will be in open states during high load conditions. By decreasing the

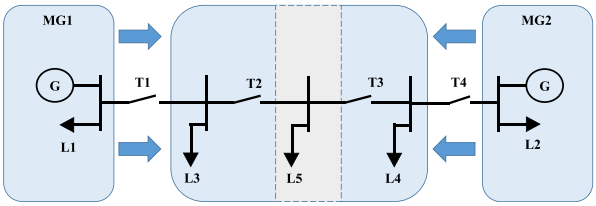

Fig. 1 MG Participation in load restoration

power consumption at off-peak hours, *T1* and *T4* will be closed to maximize the restored power by aggregating the generation capacities of the available resources in *MG1* and *MG2*. Consequently, during these intervals, loads *L3*, *L4*, and *L5* will be restored through the coupling and participation of the two MGs.

Note that for implementing the aforementioned process and recovering the maximum loads during off-peak hours, it is necessary to select the closed state for the non-flexible switches *T2* and *T3*. If the open state is chosen for them at the beginning of the period, load *L5* cannot be recovered. In addition, selecting the closed or open states for *T1* and *T4* is affected by the consumption levels of *L3*, *L4*, and *L5*, and the shared generation capacities of the MGs. Therefore, determining the state of the non-flexible switches and scheduling the operation modes of the others during a failure period could significantly affect the self-healing process.

3 The proposed restoration framework

The proposed framework for load restoration consists of two main parts. In the first part, the model regarding the topological characteristics of the distribution network is presented. In this model, the formation of dynamic MGs, the determination of their servicing areas, and deployment of coupling options are formulated in the form of linear constraints. Using a path-based algorithm, the use of different configurations through applying tie lines is also considered. In the second part, modeling of electrical features of the network, including power flow constraints and scheduling of DGs, is investigated. The formulations regarding these two parts are presented in detail in the following sections.

3.1 Topological part

The network graph considering all the buses and lines (including tie lines) is extracted. Symbols H and Λ represent the network buses (nodes) and lines (edges), respectively. In each MG, at least one DG unit, which is called the master, can fulfill the stability requirements. The root node for a MG is a bus connected to the master DG in the MG.

3.1.1 MG territory constraints

Territory constraints can be formulated as:

$$\sum_{k=1}^{N_{MGs}} \alpha_{i,k,t} \leq \quad \forall i \in H, \forall t \in T \tag{1}$$

$$\alpha_{i,k,t} \leq \sum_{\forall j \in \vartheta_{i,k}} \alpha_{j,k,t} \quad \forall i \in H, \forall j \in \vartheta_{i,k'} \forall k \in K, \forall t \in T \tag{2}$$

Equation (1) states that each node can be involved in only one of the formed MGs or none of them. If $\alpha_{i,\,k,\,t}$ is set to one, bus i at the time t belongs to MG k, while the k^{th} member from the collection H_{CDG} is considered the master. As formulated in (2), to associate a bus to an MG, at least one of its parents should be involved in that particular MG. Parents of a bus are the first buses of the existing paths between the bus and the root. For instance, in Fig. 2, the parents of node i to reach root k are m, n, p, and q.

3.1.2 Connectivity and radiality constraints

To satisfy connection and radiality constraints, the paths among the buses in each MG are analyzed. The main goal is that only one of the available paths among the buses in a MG should be set to the active state. The radiality and connectivity conditions are assured between a bus and the common node of the paths that connect the node to root of the MG. The paths between the common node and the root node are then investigated to ensure the radiality and connectivity constraints. To extract the intersection of these paths, the approach in [26] is applied. As shown in Fig. 2, these constraints are ensured for the existing paths between nodes i and ζ, and the paths between nodes ζ and k are then analyzed to satisfy the mentioned limits. Based on the above discussion, (3) and (4) can be used to validate the connectivity of bus i to its common node (node ϑ) as:

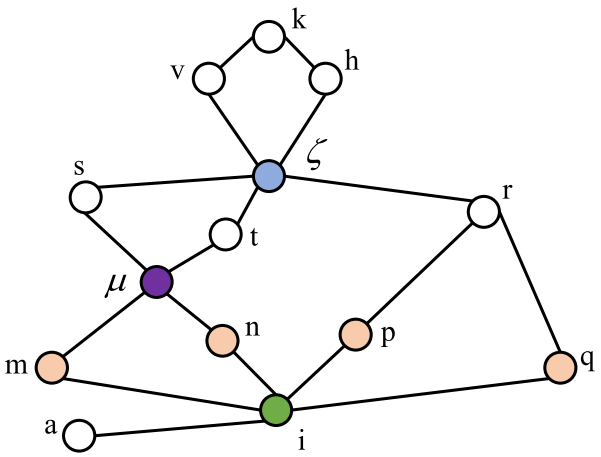

Fig. 2 A sample graph

$$\alpha_{i,k,t} \le \alpha_{\zeta,k,t} \quad \forall k \in K, \forall t \in T \tag{3}$$

$$\alpha_{i,k,t} \le \sum_{x=1}^{N_{c_{i-\zeta}}} c^{x}_{i-\zeta,t} \quad \forall x \in C_{i-\zeta}, \forall k \in K, \forall t \in T \tag{4}$$

Additionally, the state of a path is dependent on the operation mode of the lines included in that path. This issue is formulated in (5) while its linearized form is given in the Appendix.

$$c^{x}_{i-\zeta,t} = \prod_{l \in \Lambda^{x}_{i-\vartheta,t}} \beta_{l,t} \quad \forall x \in C_{i-\zeta'} \forall t \in T \tag{5}$$

In the case of several paths between buses i and ζ, only one should be considered as an active path. Thus (6) is added to avoid the loops. So to achieve radial topology, at least one of the variables indicating the line states is set to zero.

$$\sum_{l \in \Lambda^{z}_{i-\mu}} \beta_{l,t} + \sum_{\hat{l} \in \Lambda^{z}_{i-\mu}} \beta_{\hat{l},t} \le \left(L^{z}_{i-\mu} - 1\right) \quad \forall x \in C_{i-\mu'} \forall t \in T \tag{6}$$

3.1.3 Boundary constraints of MGs

The boundary constraints are shown in (7) where $\beta_{l,\ t}$ represents the state of a line and is set to zero if both sides of the line are not included in the same MG. The symbol $\odot$ represents the logical XNOR operation. The linearized form of (7) is given in the Appendix.

$$\beta_{l,t} < \alpha_{i,k,t} \odot \alpha_{j,k,t} \quad \forall l \in \Lambda, \forall i, j \in \psi_{l'} \forall k \in K, \forall t \in T \tag{7}$$

3.1.4 Failure constraints

The failure states of the lines and the nodes are formulated respectively as:

$$\beta_{l,t} < GL_l \quad \forall l \in \Lambda, \forall t \in T \tag{8}$$

$$\alpha_{i,k,t} < GB_i \quad \forall i \in H, \forall k \in K, \forall t \in T \tag{9}$$

3.1.5 Switching constraints

If a healthy line does not contain any switch, the active state is chosen for that line as shown in (10). Equation (11) demonstrates that the operation mode of the non-flexible switches does not change during the scheduling period, while the number of the allowed switching operations for the flexible types is also limited, shown by N_S in (12).

$$\beta_{l,t} \ge (1 - Sec_l) \times GL_l \quad \forall l \in \Lambda, \forall t \in T \tag{10}$$

$$\beta_{l,t} = \beta_{l,(t+1)} \quad \forall l \in \Lambda, \forall t \in \overline{T} \tag{11}$$

$$\sum_{t=1}^{T-1} u_{l,t} = N_S \quad \forall l \in \Lambda \tag{12}$$

If the auxiliary variable $u_{l,\ t}$ is equal to one, the operation mode of the available flexible switch on line l is changed between the time interval of t and $(t+1)$. This variable is defined in (13) where the symbol $\oplus$ represents the logical XOR operation.

$$u_{l,t} = \beta_{l,t} \oplus \beta_{l,(t+1)} \quad \forall l \in \Lambda, \forall t \in \overline{T} \tag{13}$$

3.2 Electrical part

3.2.1 Power balance condition for each bus

Equations (14) and (15) ensure the balance of the active and reactive powers at each node during the scheduling period as:

$$\sum_{\forall k \in K} \left[P^{DG,s}_{m,k,t} - \alpha_{i,k,t} \times D^{P}_{i,t} \right] = \sum_{\forall l \in \theta_i} \phi^{P}_{l,t} \quad \forall i \in H, \forall t \in T \tag{14}$$

$$\sum_{\forall k \in K} \left[Q^{DG,s}_{m,k,t} - \alpha_{i,k,t} \times D^{Q}_{i,t} \right] = \sum_{\forall l \in \theta_i} \phi^{Q}_{l,t} \quad \forall i \in H, \forall t \in T \tag{15}$$

3.2.2 DG constraints

Equations (16)-(18) model the DG active and reactive power limits, where node r is the connected node to DG m, as:

$$P^{DG,s}_{m,k,t} \le \alpha_{r,k,t} \times P^{DG,\ Max}_{m} \quad \forall k \in K, \forall m \in M, \forall t \in T \tag{16}$$

$$Q^{DG,s}_{m,k,t} \le \alpha_{r,k,t} \times Q^{DG,\ Max}_{m} \quad \forall k \in K, \forall m \in M, \forall t \in T \tag{17}$$

$$Q^{DG,s}_{m,k,t} \ge \alpha_{r,k,t} \times Q^{DG,\ Min}_{m} \quad \forall k \in K, \forall m \in M, \forall t \in T \tag{18}$$

3.2.3 Line flow limits

The maximum possible line flows are given as:

$$-\beta_{l,t} \times \phi^{P,\ Max}_{l} \le \phi^{P}_{l,t} \le \beta_{l,t} \times \phi^{P,\ Max}_{l} \quad \forall l \in \Lambda, \forall t \in T \tag{19}$$

$$-\beta_{l,t} \times \phi^{Q,\ Max}_{l} \le \phi^{P}_{l,t} \le \beta_{l,t} \times \phi^{Q,\ Max}_{l} \quad \forall l \in \Lambda, \forall t \in T \tag{20}$$

3.2.4 Voltage constraints

Equations (21) and (22) are the constraints regarding the actual limitations of the magnitude and phase angle of a node. It should be noted that if DG k becomes a master unit, the voltage magnitude and angle of the corresponding node are set at the controlled value of $V_{i,k,t} = \alpha_{i,k,t} \times V^{DG,set}_{k}$ and zero, respectively.

$$\alpha_{i,k,t} \times V_k^{Min} \le V_{i,k,t} \le \alpha_{i,k,t} \times V_k^{Max} \quad \forall i \in H, \forall k \in K, \forall t \in T \tag{21}$$

$$-\alpha_{i,k,t} \times \delta^{Max} \le \delta_{i,k,t} \le \alpha_{i,k,t} \times \delta^{Max} \quad \forall i \in H, \forall k \in K, \forall t \in T \tag{22}$$

3.2.5 Power flow constraints

The method in [27] is used to conduct the load flow calculations. As stated in [27], linearized equations of power flow in electric distribution systems can be formulated as:

$$F1_l = \frac{r_l}{r_l^2 + x_l^2} \quad , \quad F2_l = \frac{x_l}{r_l^2 + x_l^2} \tag{23}$$

$$\phi_{l,t}^P = \tilde{\phi}_{l,t}^P + \sum_{\forall k \in K} \left[\left(\delta_{j,k,t} - \delta_{i,k,t} \right) \times F2_l + \left(V_{j,k,t} - V_{i,k,t} \right) \times F1_l \right] \forall i \in H, \forall t \in T \tag{24}$$

$$\phi_{l,t}^Q = \tilde{\phi}_{l,t}^Q + \sum_{\forall k \in K} \left[\left(\delta_{i,k,t} - \delta_{j,k,t} \right) \times F1_l + \left(V_{j,k,t} - V_{i,k,t} \right) \times F2_l \right] \forall i \in H, \forall t \in T \tag{25}$$

Equations (26) and (27) show the slack variable limits to make equality constraints valid when the nodes of a line are not involved in the same MG.

$$-\left(1-\beta_{l,t}\right) \times E \le \tilde{\phi}_{l,t}^P \le \left(1-\beta_{l,t}\right) \times E \quad \forall l \in \Lambda, \forall t \in T \tag{26}$$

$$-\left(1-\beta_{l,t}\right) \times E \le \tilde{\phi}_{l,t}^Q \le \left(1-\beta_{l,t}\right) \times E \quad \forall l \in \Lambda, \forall t \in T \tag{27}$$

3.2.6 Objective function

Maximizing the total amount of the recovered loads considering their priorities is the objective function of the restoration problem, i.e.:

$$Max : ObjF = \sum_{t \in T} \sum_{\forall i \in N} \left(Pr_{i,t}^L \times D_{i,t}^P \times \sum_{\forall k \in K} \alpha_{i,k,t} \right) \tag{28}$$

3.3 Solution methodology

The Benders' decomposition approach [28] is adopted to decouple the topological and electrical parts in the optimization. The topological part is considered the master problem (MP), where the states of the network nodes and lines, open and closed statuses of the flexible and non-flexible switches, and MG configurations are determined. The electrical part is then assumed to be the sub-problem (SP) and is evaluated after determining the topological variables in the MP. The fitness values of the SP are sent back to the MP through generating Benders cuts. For better clarification of the procedure, the flowchart of the proposed optimal recovery model is depicted in Fig. 3.

The original optimization problem is decoupled into an MP and an SP. The MP is formulated as:

$$\begin{aligned} &Minimize\ Z_{lower} \\ &Z_{lower} \ge -\sum_{t \in T} \sum_{\forall i \in N} \left(Pr_{i,t}^L \times D_{i,t}^P \times \sum_{\forall k \in K} \alpha_{i,k,t} \right) \\ &s.t.\ \ (1)-(13) \end{aligned} \tag{29}$$

Equation (29) provides an initial lower bound solution: $\hat{Z}_{lower}$ at $\hat{\alpha}$ and $\hat{\beta}$ (set of the topological binary variables). The results of the MP are introduced to the SP for minimizing load curtailments at each MG and satisfying the network constraints. By introducing the auxiliary variables γ, the SP can be written as Eq. (30).

$$\begin{aligned} &Minimize\ w = \sum_{t \in T} \sum_{\forall i \in N} \left(D_{i,t}^P \times \sum_{\forall k \in K} \gamma_{i,k,t} \right) \\ &s.t. \\ &0 \le \gamma_{i,k,t} \le \hat{\alpha}_{i,k,t} \\ &\sum_{\forall k \in K} \left[P_{m,k,t}^{DG,s} - \left(\hat{\alpha}_{i,k,t} - \gamma_{i,k,t} \right) \times D_{i,t}^P \right] = \sum_{\forall l \in \theta_i} \phi_{l,t}^P \\ &\forall i \in H, \forall t \in T \\ &\sum_{\forall k \in K} \left[Q_{m,k,t}^{DG,s} - \left(\hat{\alpha}_{i,k,t} - \gamma_{i,k,t} \right) \times D_{i,t}^Q \right] = \sum_{\forall l \in \theta_i} \phi_{l,t}^Q \\ &\forall i \in H, \forall t \in T \\ &(16)-(27) \textit{and fixed } \hat{\alpha} \textit{ and } \hat{\beta}. \end{aligned} \tag{30}$$

The solution of the optimal SP measures the variations in the objective function. This SP forms the corresponding Benders cut, which is added to the MP for solving the next iteration of the problem. The optimality cut associated with the nth trial solution is formulated as Eq. (31).

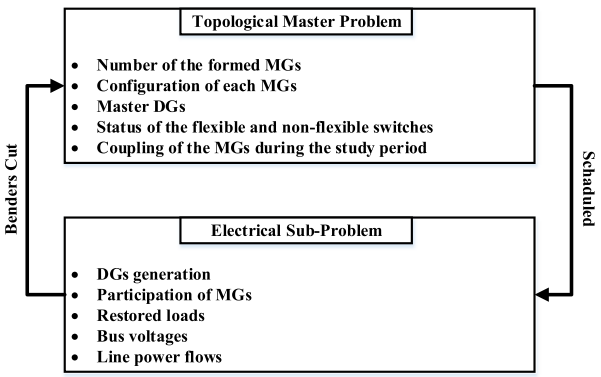

Fig. 3 Decoupling the topological and electrical parts of the problem

$$
\begin{aligned}
Z_{lower} \geq & -\sum_{t\in T}\sum_{\forall i\in N}\left(Pr_{i,t}^{L}\times D_{i,t}^{P}\times\sum_{\forall k\in K}\alpha_{i,k,t}\right)\\
& +w^{n}+\sum_{t\in T}\sum_{\forall m\in M}\sum_{\forall k\in K}\left(\bar{\pi}_{m,k,t}^{n,DG-p}\times P_{m}^{DG,\,Max}\times\left[\alpha_{r,k,t}-\hat{\alpha}_{r,k,t}^{n}\right]\right)\\
& +\sum_{t\in T}\sum_{\forall m\in M}\sum_{\forall k\in K}\left(\left(\bar{\pi}_{m,k,t}^{n,DG-q}\times Q_{m}^{DG,\,Max}-\underline{\pi}_{m,k,t}^{n,DG-q}\times Q_{m}^{DG,\,Max}\right)\right.\\
& \left.\times\left[\alpha_{r,k,t}-\hat{\alpha}_{r,k,t}^{n}\right]\right)+\sum_{t\in T}\sum_{\forall l\in\Lambda}\left(\left(\bar{\pi}_{l,t}^{n,l-p}+\underline{\pi}_{l,t}^{n,l-p}\right)\times\phi_{l}^{P,\,Max}\times\left[\beta_{l,t}-\hat{\beta}_{l,t}^{n}\right]\right)\\
& +\sum_{t\in T}\sum_{\forall l\in\Lambda}\left(\left(\bar{\pi}_{l,t}^{n,l-q}+\underline{\pi}_{l,t}^{n,l-q}\right)\times\phi_{l}^{Q,\,Max}\times\left[\beta_{l,t}-\hat{\beta}_{l,t}^{n}\right]\right)\\
& +\sum_{t\in T}\sum_{\forall i\in H}\sum_{\forall k\in K}\left(\left(\bar{\pi}_{i,k,t}^{n,V}\times V^{Max}-\underline{\pi}_{i,k,t}^{n,V}\times V^{Min}\right)\times\left[\alpha_{i,k,t}-\hat{\alpha}_{i,k,t}^{n}\right]\right)\\
& +\sum_{t\in T}\sum_{\forall i\in H}\sum_{\forall k\in K}\left(\left(\bar{\pi}_{i,k,t}^{n,\delta}-\underline{\pi}_{i,k,t}^{n,\delta}\right)\times\delta^{Max}\times\left[\alpha_{i,k,t}-\hat{\alpha}_{i,k,t}^{n}\right]\right)\\
& -\sum_{t\in T}\sum_{\forall l\in\Lambda}\left(\left(\bar{\pi}_{l,t}^{n,zl-p}+\underline{\pi}_{l,t}^{n,zl-p}\right)\times E\times\left[\beta_{l,t}-\hat{\beta}_{l,t}^{n}\right]\right)\\
& -\sum_{t\in T}\sum_{\forall l\in\Lambda}\left(\left(\bar{\pi}_{l,t}^{n,zl-q}+\underline{\pi}_{l,t}^{n,zl-q}\right)\times E\times\left[\beta_{l,t}-\hat{\beta}_{l,t}^{n}\right]\right)
\end{aligned}
\tag{31}
$$

where n is the current number of iterations, and $\bar{\pi}_{m,k,t}^{n,DG-p}$, $\bar{\pi}_{m,k,t}^{n,DG-q}$, $\underline{\pi}_{m,k,t}^{n,DG-q}$, $\bar{\pi}_{l,t}^{n,l-p}$, $\underline{\pi}_{l,t}^{n,l-p}$, $\bar{\pi}_{l,t}^{n,l-q}$, $\underline{\pi}_{l,t}^{n,l-q}$, $\bar{\pi}_{i,k,t}^{n,V}$, $\underline{\pi}_{i,k,t}^{n,V}$, $\bar{\pi}_{i,k,t}^{n,\delta}$, $\underline{\pi}_{i,k,t}^{n,\delta}$, $\bar{\pi}_{l,t}^{n,zl-p}$, $\underline{\pi}_{l,t}^{n,zl-p}$, $\bar{\pi}_{l,t}^{n,zl-q}$, $\underline{\pi}_{l,t}^{n,zl-q}$ are the multiplier values at the nth iteration, representing the incremental changes in the optimal objective. The solution of the SP provides an upper bound for the original problem:

$$
\begin{aligned}
Z_{lower} = & -\sum_{t\in T}\sum_{\forall i\in N}\left(Pr_{i,t}^{L}\times D_{i,t}^{P}\times\sum_{\forall k\in K}\hat{\alpha}_{i,k,t}\right)\\
& +\hat{w}
\end{aligned}
\tag{32}
$$

Defined lower and upper bounds can be used to create an effective convergence criterion. The process repeats until a converged optimal solution is found, i.e., when the optimal value of the SP (w) is as small as a preset threshold value.

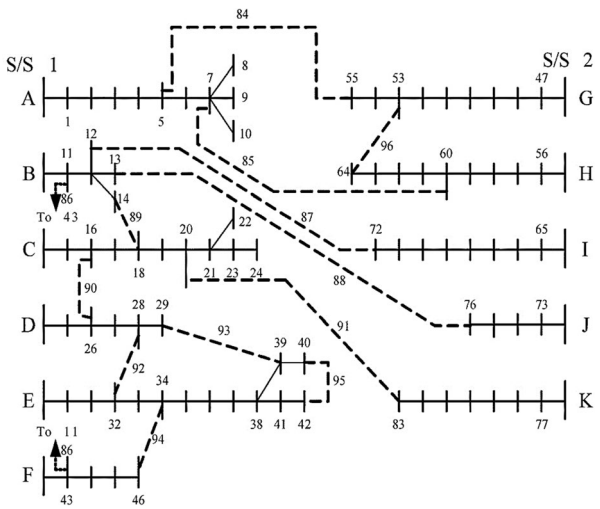

Fig. 4 Single line diagram of the test network

Table 1 Required information about the DGs

Unit	Bus	Cap. (kW)	Q^{max} (kvar)	Q^{min} (kvar)
DG1	7	2400	2000	− 2000
DG2	20	3000	2400	− 2400
DG3	26	2600	2100	− 2100
DG4	53	2000	1650	− 1650
DG5	71	2500	1900	− 1900

4 Simulation results

The efficiency of the proposed model is investigated in this section. The simulations are programmed with MATLAB software and solved using the CPLEX solver, all conducted on a PC with Intel Core i7 CPU @4 GHz and 16 GB RAM, considering a gap of 0.02% as a convergence criterion.

4.1 Test network

The proposed model is applied to an 11.4 kV modified 84-bus test system depicted in Fig. 4 [29], with total real and reactive power consumptions of 28.350 MW and 20.70 MVar, respectively. The network consists of 11 feeders, 84 buses, 96 lines, 13 flexible and 48 non-flexible switches. The flexible switches are located on the tie lines. Detailed information about the load consumptions, line parameters, and switch locations are given in (https://www.dropbox.com/s/aeznll8on2t6e9l/modified-84BusSystem-Data.xlsx?dl=0)].

In addition, five DG units, with the ability to act as a master unit, are installed in this network. Therefore, a maximum of five MGs could be formed in this system. The required data on the installed DGs are given in Table 1. Figure 5 illustrates the consumption data for 1 day based on P.U. values, and the loads are considered as having equal priority. It is also assumed that the main sub-station is in the failure state (the buses with letters are all connected to this sub-station) because of a severe

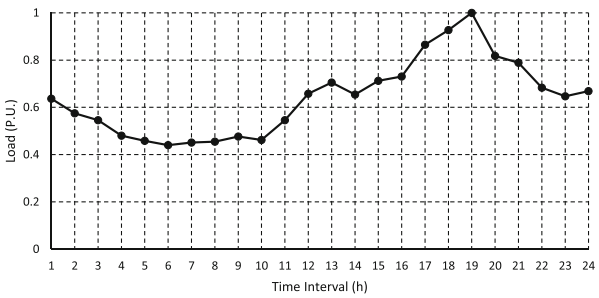

Fig. 5 Daily load profile [30]

Table 2 Impact of applying different strategies

	St1	St2	St3	St4	St5	St6
Exe. Time (sec)	0.176	0.179	0.179	0.923	1.017	0.749
No. MGs	5	5	5	5	2	2
Master DGs	1, 2, 3, 4, 5	1, 2, 3, 4, 5	1, 2, 3, 4, 5	1, 2, 3, 4, 5	1, 5	1, 3
Restored Energy (10^5 kWh)	1.39	1.65	1.94	1.53	1.92	2.3
Recovery Index	0.397	0.472	0.557	0.437	0.549	0.658

event. The failure condition, in this case, lasts 18 h (from 13:00 to 07:00).

4.2 Case I: impact of tie lines and DGs

In this case, six different strategies are implemented, and their impacts on the self-healing process are examined. These strategies are as follows:

- St1: no Tie & 100% DG
- St2: no Tie & 125% DG
- St3: no Tie & 150% DG
- St4: with Tie & 100% DG
- St5: with Tie & 100% DG
- St6: with Tie & 100% DG

MG coupling is not considered in this case, and all switches are assumed to be non-flexible types. The detailed results for each strategy are listed in Table 2.

The recovery index is the ratio of the recovered load consumptions to the system's whole electric energy consumption during the study period. From the results, proper use of the generation along with the switching capabilities can significantly improve system functionality after the occurrence of the severe event. For instance, the recovery index increases to around 65% in strategy 6, using 150% capacity of DG units and applying tie lines.

These results accentuate the importance of optimal allocation of the technologies in the distribution networks.

The results show that a proper strategy based on cost-benefit analysis should be adopted to enhance restoration capability. For example, in the test network, the system recovery index improves 9% by a 25% increase of the DG capacity in strategy 2, while applying the tie lines in strategy 4 increases the ability by 5%. Also, by employing the tie lines in strategies 4, 5 and 6, more flexibility is achieved, and the number of the formed MGs is also decreased. The formed MGs in strategy 4 are depicted in Fig. 6. The obtained simulation execution times reported in Table 2**.** Confirm the computability and efficiency of the proposed algorithm.

4.3 Case II: impact of MG coupling

The participation of MGs in load restoration during the failure period is now investigated. The impact of applying MG coupling in strategies 4, 5, and 6 are stated in Table 3. In Mode 1, coupling is not used, and in Mode 2, coupling is applied.

Based on the results, with MG participation, system recovery in strategies 4, 5 and 6 is improved by around 14%, 16%, and 17%, respectively. The improvement in the recovered energy is due to the fact that, without employing coupling options, only one configuration could be implemented for MG formation. However, by considering flexible switching, different dynamic structures are used and consequently more benefits are attained. For a better explanation, scheduling of MGs in the self-healing process regarding the tie lines and full capacity of DGs (strategy 4) is analyzed. Three different configurations are selected for MG formation in feeders A, G, and H, while the structures in feeders A, G, and H are depicted in Fig. 7. Nine structures are obtained to form and couple the MGs on the other part of the network (feeders B, C, D, E, F, I, J, K).

As shown in Fig. 7, three configurations are chosen in the study period with the proposed optimization approach. Because of low power consumption during the first interval (between 13:00 and 17:00), only one MG is formed, and structure I is selected for supplying the loads connected to feeders A, G, and H. In this structure, tie

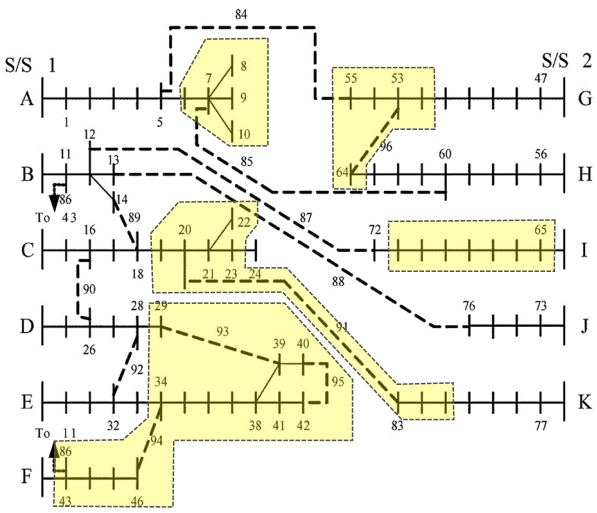

Fig. 6 Formed MGs in strategy 4

Table 3 Impact of MG Coupling

	St4		St5		St6	
Mode	**1**	**2**	**1**	**2**	**1**	**2**
Recovered Energy (10^5 kWh)	1.53	2.01	1.92	2.45	2.3	2.9
Recovery Index	0.437	0.573	0.549	0.701	0.658	0.829

lines 84, 85, and 96 are in the closed state. At the second interval (between 17:00 and 18:00), by opening the flexible switch located on tie-line 84, and disconnecting loads L1 to L5, the formed MG in the previous interval becomes smaller, and structure II is employed, i.e., flexible switching capabilities are used for load management in this interval to achieve power balance in the MG.

Because of high power consumption in the third interval (between 18:00 to 21:00), by applying structure III and opening tie lines 84 and 96, the mentioned MG is decoupled into two smaller MGs. Therefore, DG1 and DG4 are the master units in this time interval. Because of the decreased loads during the fourth interval (between 21:00 to 22:00) and the closing tie lines 85 and 96, structure II is used once again and the two MGs are joined together. At the next intervals (between 22:00 to 07:00), tie line 84 is closed and structure I is employed again.

The impact of MG coupling on the recovered energy and the recovery index at each time interval during the study period are depicted in Figs. 8 and 9, respectively.

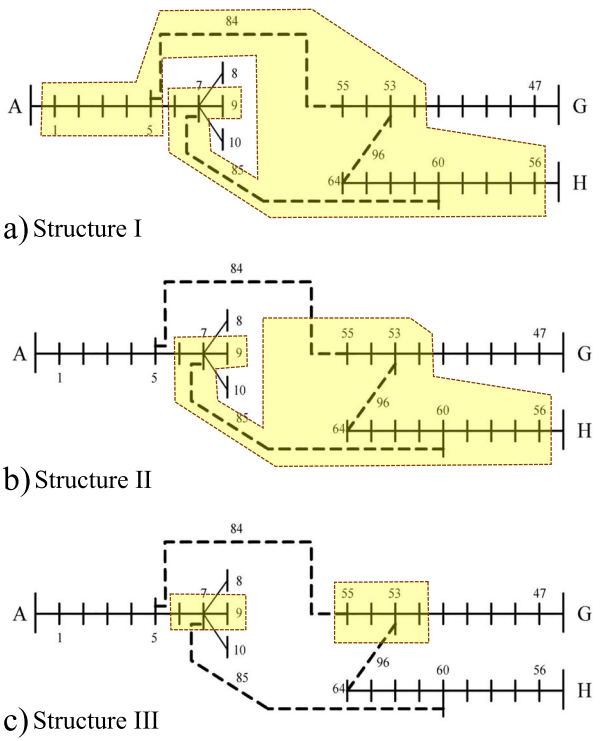

Fig. 7 MG configurations during the period

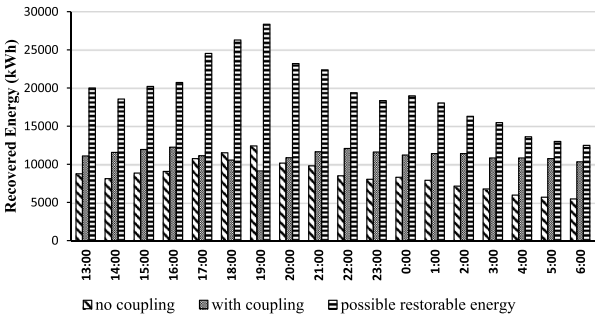

Fig. 8 Restored energy in each hour

As can be seen, by enhancing system functionality through flexible switching and realizing MG coupling, the restored energy, specifically during the low power consumption hours, is increased, and more benefits are attained.

The lower recovery index for the period of 18:00 to 20:00 is due to the switching limits of the non-flexible switches. This indicates that the proposed approach sets the statuses of the non-flexible switches to improve the performance of the system, even at the cost of losing some of the benefits during the mentioned intervals. This highlights the importance of the optimal placement of the flexible and non-flexible switches in the distribution networks.

4.4 Comparing the efficiency

In this subsection, the convergence data of the proposed algorithm based on Benders' decomposition is provided and the results are compared to those using the genetic algorithm (GA) proposed in [31], as shown in Figs. 10 and 11, and Table 4.

The GA method is implemented in MATLAB software, and its population, crossover, and mutation parameters are set to 100, 0.6, and 0.2, respectively. Strategy 4 in Case-I, which employs the tie-lines and 100% capacity of DGs, is considered for the comparison. As can be seen, the acquired results from the two

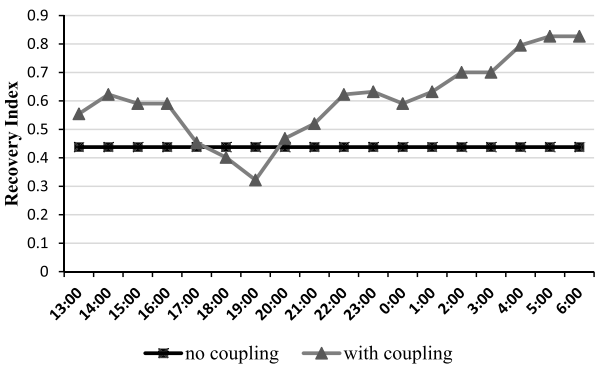

Fig. 9 Recovery index in each hour

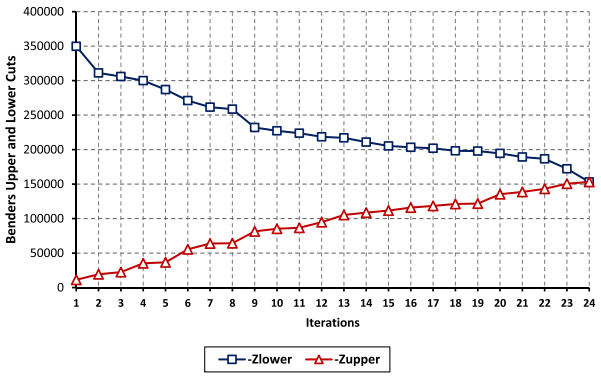

Fig. 10 Benders' decomposition convergence diagram

approaches are quite close. However, the proposed approach is much faster, making it more attractive for practical application, especially when the grid size and the number of optimization parameters are large.

5 Conclusion

In this paper, a load restoration process in distribution networks after a severe event is presented. The formation of MGs and their participation in load sharing during the failure period are formulated as a MILP optimization problem. To model the system topological characteristics, a novel linear approach that considers the network paths is proposed. The Benders' decomposition approach is used to enhance computability. The impact of different items such as switching capabilities, DGs capacities, and coupling of MGs on the self-healing process are investigated. The simulation results show that the flexible switching and MG coupling capability can lead to more efficiency and improve system performance when dealing with such events. The proposed model properly employs coupled MGs to enhance the system recovery considerably. Incorporating other technologies, such as demand response programs and electric vehicles, and optimal placement of flexible switches to enhance coupling proficiency are considered for future work.

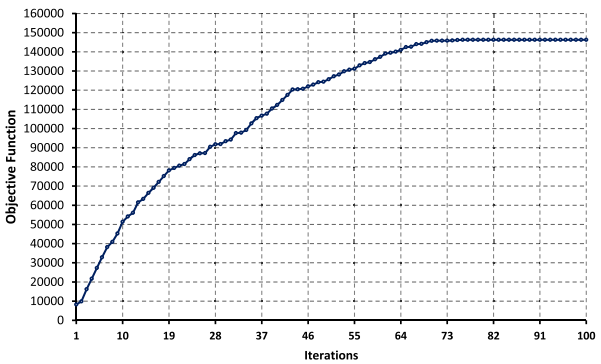

Fig. 11 GA convergence diagram

Table 4 Comparison results

Method	Best Result	Number of Iterations
GA	146,280.4	71
Benders	153,120	24

6 Nomenclature

i Node index
k MGs index
m DGs index
Λ Collection of the network lines
H Collection of the network buses
K Collection of the formable MGs
M Collection of the DGs
θ_i Connected lines to the bus i
Ψ_l Buses connected to the line l
E A very big number
ζ Lowest common node of the parents
H_{ADG} Connected buses to the DGs
H_{CDG} Connected buses to the controllable DGs
$C_{i-\mu}$ Available paths between bus i and μ
N_{CDG} Number of the controllable DGs
N_{MGs} Number of the MGs that can be formed
$D^P_{i,t}$ Consumption for the bus i at hour t
L^a_{b-c} Number of the lines in the path $\Lambda^a_{b-c,t}$
δ^{Max} Maximum limit of the voltage angles
$\beta_{l,\,t}$ Connection status of the line l
GB_i Failure status of the node i after the disaster
GL_l Failure status of line l after the disaster
$\alpha_{i,\,k,\,t}$ Connection status of the bus i
$\delta_{i,\,k,\,t}$ Phase of the voltage for the bus i
$V_{i,\,k,\,t}$ Magnitude of the voltage for the bus i
Sec_l Availability of a switch on the line l
$c^a_{b-c,t}$ Status of the path a from bus b to c
$N_{c_{a-b}}$ Number of paths from the bus a to b
$\Lambda^a_{b-c,t}$ Lines of the path a from bus b to c
r_l, x_l Electrical features of the line l
$V^{DG,set}_k$ Voltage set point for the DG m
$\phi^P_{l,t}$ Active flows of the line l
$\phi^q_{l,t}$ Reactive flows of the line l
$P^{DG,s}_{m,k,t}$ Active power of the DG m
$Q^{DG,s}_{m,k,t}$ Reactive power of the DG m
$P^{DG,\,Max}_m$ Active power limits of DG m
$Q^{DG,\,Max}_m$ Maximum reactive power of DG m
$Q^{DG,\,Min}_m$ Minimum reactive power of DG m
$\tilde{\phi}^P_{l,t}$ Auxiliary variables
$\tilde{\phi}^q_{l,t}$ Auxiliary variables

$\phi_l^{P,\,Max}$ Active power flow limits of the line l
$\phi_l^{Q,\,Max}$ Reactive power limits of the line l

7 Appendix

a) Linearized form of (5) is given as:

$$c^x_{i-\zeta,t} \le \beta_{l,t} \quad \forall x \in C_{i-\zeta}, \forall l \in \Lambda^x_{i-\zeta,t}, \forall t \in T \tag{33}$$

$$c^x_{i-\zeta,t} \ge \sum_{l \in \Lambda^x_{i-\zeta,t}} \beta_{l,t} - \left(L^x_{i-\zeta} - 1\right) \quad \forall x \in C_{i-\zeta}, \forall t \in T \tag{34}$$

b) Auxiliary binary variables $\varkappa_{l,\,k,\,t}$ and $\hat{\varkappa}_{l,k,t}$ are defined to linearize (7) as:

$$\beta_{l,t} < \varkappa_{l,k,t} + \hat{\varkappa}_{l,k,t} \quad \forall l \in \Lambda, \forall k \in K, \forall t \in T \tag{35}$$

$$\begin{cases} \varkappa_{l,k,t} \le \alpha_{i,k,t} \\ \varkappa_{l,k,t} \le \alpha_{j,k,t} \\ \varkappa_{l,k,t} \ge \alpha_{i,k,t} + \alpha_{j,k,t} - 1 \end{cases} \tag{36}$$
$$\forall i, j \in \Psi_l, \forall l \in \Lambda, \forall k \in K, \forall t \in T$$

$$\begin{cases} \hat{\varkappa}_{l,k,t} \le 1 - \alpha_{i,k,t} \\ \hat{\varkappa}_{l,k,t} \le 1 - \alpha_{j,k,t} \\ \hat{\varkappa}_{l,k,t} \ge 1 - \alpha_{i,k,t} - \alpha_{j,k,t} \end{cases} \tag{37}$$
$$\forall i, j \in \Psi_l, \forall l \in \Lambda, \forall k \in K, \forall t \in T$$

c) Auxiliary binary variables $\rho_{l,\,t}$ and $\hat{\rho}_{l,t}$ are defined to linearize (13) as:

$$u_{l,t} \le \rho_{l,t} + \hat{\rho}_{l,t} \quad \forall l \in \Lambda, \forall t \in \overline{T} \tag{38}$$

$$\begin{cases} \rho_{l,t} \le \beta_{l,t} \\ \rho_{l,t} \le 1 - \beta_{l,t+1} \\ \rho_{l,t} \ge \beta_{l,t} - \beta_{l,t+1} \end{cases} \tag{39}$$
$$\forall l \in \Lambda, \forall t \in \overline{T}$$

$$\begin{cases} \rho_{l,t} \le \beta_{l,t+1} \\ \rho_{l,t} \le 1 - \beta_{l,t} \\ \rho_{l,t} \ge \beta_{l,t+1} - \beta l, t \end{cases} \tag{40}$$
$$\forall l \in \Lambda, \forall t \in \overline{T}$$

Acknowledgements
Not applicable.

Authors' contributions
S M did the analysis of data and was in charge of running different simulations and writing the paper. A A was in charge of collecting the necessary data for analysis and simulations, doing literature review, and writing the article. S R M participated in the overall design of the work and running simulations and interpreting the results and finally M R H made contributions in the concepts and idea and final preparation of the article. The author(s) read and approved the final manuscript.

Funding
There is no funding for this article.

Availability of data and materials
The datasets used and/or analysed during the current study are available from the corresponding author on reasonable request.

Declaration

Competing interests
The authors declare that they have no known competing financial interests or personal relationships that could have appeared to influence the work reported in this paper.

Author details
[1]Faculty of Electrical and Computer Engineering, Tarbiat Modares University, PO Box 14115-111, Tehran, Iran. [2]Skolkovo Institute of Science and Technology (Skoltech), Moscow, Russia. [3]Department of Electrical Engineering, University of Torbat Heydarieh, Torbat Heydarieh, Iran.

Received: 27 October 2020 Accepted: 11 May 2021
Published online: 29 July 2021

References

1. Bird, S., & Hotaling, C. (2018). Multi-stakeholder microgrids for resilience and sustainability. *Environmental Hazards*, *16*(2), 116–132.
2. Zidan, A., Khairalla, M., Abdrabou, A. M., Khalifa, T., Shaban, K., Abdrabou, A., … Gaouda, A. M. (2016). Fault detection, isolation, and service restoration in distribution systems: State-of-the-art and future trends. *IEEE Transactions on Smart Grid*, *8*(5), 2170–2185.
3. Liu, Y., Fan, R., & Terzija, V. (2016). Power system restoration: A literature review from 2006 to 2016. *Journal of Modern Power Systems and Clean Energy*, *4*(3), 332–341. https://doi.org/10.1007/s40565-016-0219-2.
4. Gururajapathy, S. S., Mokhlis, H., & Illias, H. A. (2017). Fault location and detection techniques in power distribution systems with distributed generation: A review. *Renewable and sustainable energy reviews*, *74*, 949–958.
5. Jamali, S., Bahmanyar, A., & Ranjbar, S. (2020). Hybrid classifier for fault location in active distribution networks. *Protection and Control of Modern Power Systems*, *5*(1), 1–9.
6. Chen, C., Wang, J., & Ton, D. (2017). Modernizing distribution system restoration to achieve grid resiliency against extreme weather events: An integrated solution. *Proceedings of the IEEE*, *105*(7), 1267–1288. https://doi.org/10.1109/JPROC.2017.2684780.
7. Alahyari, A., Ehsan, M., Pozo, D., & Farrokhifar, M. (2020). Hybrid uncertainty-based offering strategy for virtual power plants. *IET Renewable Power Generation*, *14*(13), 2359–2366. https://doi.org/10.1049/iet-rpg.2020.0249.
8. Injeti, S. K., & Thunuguntla, V. K. (2020). Optimal integration of DGs into radial distribution network in the presence of plug-in electric vehicles to minimize daily active power losses and to improve the voltage profile of the system using bio-inspired optimization algorithms. *Protection and Control of Modern Power Systems*, *5*(1), 1–15.

9. Chandak, S., Bhowmik, P., & Rout, P. K. (2019). Load shedding strategy coordinated with storage device and D-STATCOM to enhance the microgrid stability. *Protection and Control of Modern Power*, *4*(1), 1–19.
10. Alahyari, A., & Pozo, D. (2019). Online demand response for end-user loads. In *2019 IEEE Milan PowerTech*. IEEE.
11. Ding, T., Lin, Y., Bie, Z., & Chen, C. (2017). A resilient microgrid formation strategy for load restoration considering master-slave distributed generators and topology reconfiguration. *Applied Energy*, *199*, 205–216.
12. Chavali, S., Pahwa, A., & Das, S. (2004). Evolutionary approaches for the optimal restoration of sections in distribution systems. *Electric Power Components and Systems*, *32*(9), 869–881. https://doi.org/10.1080/15325000490253560.
13. Ćurčić, S., Özveren, C. S., Crowe, L., & Lo, P. K. L. (1995). Electric power distribution network restoration: A survey of papers and a review of the restoration problem. *Electric Power Systems Research*, *35*(2), 73–86. https://doi.org/10.1016/0378-7796(95)00991-4.
14. Xiaoyu, H., Mingchao, X., & Yinghui, H. (2014). A service restoration method for active distribution network. *Energy Procedia*, *61*, 339–344.
15. Chen, W.-H. (2010). Quantitative decision-making model for distribution system restoration. *IEEE Transactions on Power Systems*, *25*(1), 313–321. https://doi.org/10.1109/TPWRS.2009.2036811.
16. Ju, L., Zhang, Q., Tan, Z., Wang, W., He, X., & Zhang, Z. (2018). Multi-agent-system-based coupling control optimization model for micro-grid group intelligent scheduling considering autonomy-cooperative operation strategy. *Energy*, *157*, 1035–1052.
17. Lv, T., & Ai, Q. (2016). Interactive energy management of networked microgrids-based active distribution system considering large-scale integration of renewable energy resources. *Applied Energy*, *163*, 408–422.
18. Che, L., Khodayar, M., & Shahidehpour, M. (2014). Only connect: Microgrids for distribution system restoration. *IEEE Power and Energy Magazine*, *12*(1), 70–81.
19. Feng, X., Shekhar, A., Yang, F., & E. Hebner R, Bauer P. (2017). Comparison of hierarchical control and distributed control for microgrid. *Electric Power Components and Systems*, *45*(10), 1043–1056. https://doi.org/10.1080/15325008.2017.1318982.
20. Hussain, A., Bui, V.-H., & Kim, H.-M. (2019). Microgrids as a resilience resource and strategies used by microgrids for enhancing resilience. *Applied Energy*, *240*, 56–72.
21. Li, Z., Shahidehpour, M., Aminifar, F., Alabdulwahab, A., & Al-Turki, Y. (2017). Networked microgrids for enhancing the power system resilience. *Proceedings of the IEEE*, *105*(7), 1289–1310.
22. Gao, H., Chen, Y., Xu, Y., & Liu, C.-C. (2016). Resilience-oriented critical load restoration using microgrids in distribution systems. *IEEE Transactions on Smart Grid*, *7*(6), 2837–2848. https://doi.org/10.1109/TSG.2016.2550625.
23. Ferdous, S. M., Shafiullah, G. M., Shahnia, F., Elavarasan, R. M., & Subramaniam, U. (2020). Dynamic frequency and overload management in autonomous coupled microgrids for self-healing and resiliency improvement. *IEEE Access*, *8*, 116796–116811.
24. Wang, Z., & Wang, J. (2017). Service restoration based on AMI and networked MGs under extreme weather events. *IET Generation, Transmission & Distribution*, *11*, 401–408.
25. Chen, C., Wang, J., Qiu, F., & Zhao, D. (2016). Resilient distribution system by microgrids formation after natural disasters. *IEEE Transactions on Smart Grid*, *7*(2), 958–966. https://doi.org/10.1109/TSG.2015.2429653.
26. Fischer, J., & Heun, V. (2006). Theoretical and practical improvements on the RMQ-problem, with applications to LCA and LCE. In *CPM*, (vol. 6, pp. 36–48).
27. Yuan, H., Li, F., Wei, Y., & Zhu, J. (2016). Novel linearized power flow and linearized OPF models for active distribution networks with application in distribution LMP. *IEEE Transactions on Smart Grid, 9*(1), 438–448.
28. Rahmaniani, R., Crainic, T. G., Gendreau, M., & Rei, W. (2016). The Benders decomposition algorithm: A literature review. *European Journal of Operational Research , 259*(3), 801–817.
29. Chiou, J.-P., Chang, C.-F., & Ching-Tzong, S. (2005). Variable scaling hybrid differential evolution for solving network reconfiguration of distribution systems. *IEEE Transactions on Power Systems*, *20*(2), 668–674. https://doi.org/10.1109/TPWRS.2005.846096.
30. Beatty, S. J., Wild, P., & Buckham, B. J. (2010). Integration of a wave energy converter into the electricity supply of a remote Alaskan island. *Renewable Energy*, *35*(6), 1203–1213. https://doi.org/10.1016/j.renene.2009.11.040.
31. Molaali, M., & Abedi, M. (2018). A new heuristic method for distribution network restoration and load elimination using genetic algorithm. In *2018 Electrical Power Distribution Conference (EPDC)*, (pp. 46–51). IEEE.